Accepted Manuscript

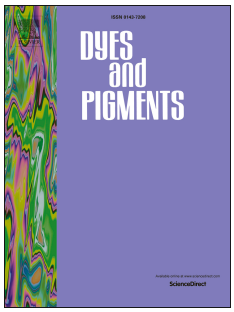

A fully-aqueous red-fluorescent probe for selective optical sensing of Hg^{2+} and its application in living cells

Murali Krishna Pola, Mandapati V. Ramakrishnam Raju, Chein-Ming Lin, Raghunath Putikam, Ming-Chang Lin, Chandra Prakash Epperla, Huan-Cheng Chang, San-Yuan Chen, Hong-Cheu Lin

PII: S0143-7208(16)30087-0

DOI: 10.1016/j.dyepig.2016.03.028

Reference: DYPI 5153

To appear in: *Dyes and Pigments*

Received Date: 21 January 2016

Revised Date: 13 March 2016

Accepted Date: 14 March 2016

Please cite this article as: Pola MK, Ramakrishnam Raju MV, Lin C-M, Putikam R, Lin M-C, Epperla CP, Chang H-C, Chen S-Y, Lin H-C, A fully-aqueous red-fluorescent probe for selective optical sensing of Hg^{2+} and its application in living cells, *Dyes and Pigments* (2016), doi: 10.1016/j.dyepig.2016.03.028.

Graphical Abstract

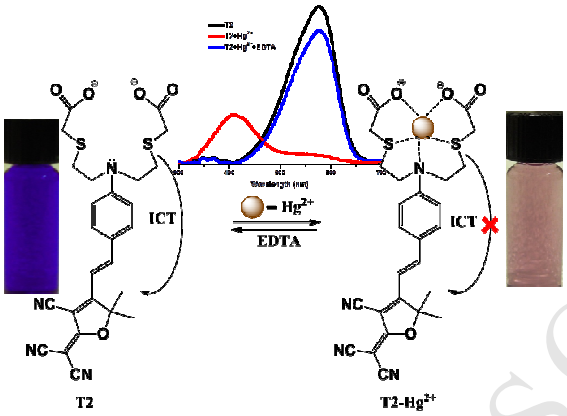

A fully-aqueous red-fluorescent probe for selective optical sensing of Hg^{2+} and its application in living cells

Murali Krishna Pola,[a] Mandapati V. Ramakrishnam Raju,[a] Chein-Ming Lin,[a] Raghunath Putikam,[b] Ming-Chang Lin,[b] Chandra Prakash Epperla,[c] Huan-Cheng Chang,[c] San-Yuan Chen, [a] Hong-Cheu Lin[a,*]

[a] Department of Materials Science and Engineering, National Chiao Tung University, Hsinchu 300, Taiwan.

[b] Center for Interdisciplinary Molecular Science, Department of Applied Chemistry, National Chiao Tung University, Hsinchu 300, Taiwan.

[c] Institute of Atomic and Molecular Sciences, Academia Sinica, Taipei 106, Taiwan.

Supporting Information Placeholder

KEYWORDS: aqueous medium; push-pull chromophore; ICT, living cell.

Abstract

A new red-fluorescent mercury ion sensor material is designed and synthesized, which is composed of a tweezer-shaped hydrophilic probe containing bifurcated soft-base atoms N and S coupled with 2-dicyanomethylene-3-cyano-4,5,5-trimethyl-2,5-dihydrofuran (TCF) unit. By virtue of the strong electron-accepting nature of TCF unit (as a push-pull chromophore), this designed sensor material can selectively detect Hg^{2+} over various tested metal ions in a 100% aqueous medium via naked-eye and photoluminescence (PL) observations. Theoretical and time-resolved photoluminescence measurements further confirmed the selectivity and reversibility of the probe towards Hg^{2+} via intramolocular charge transfer mechanism in this sensor material. Moreover, the living cell tests by confocal fluorescence images of this sensor material towards Hg^{2+} were also investigated. Finally, distinguished absorption changes and fluorescence quenching spectral appearances allowed us to present the selective optical indicator of Hg^{2+} via TCF moiety for the first time.

1. Introduction

Despite the vital roles of many metal ions in sustaining life, it is required to have precise control to maintain an ecological balance in living cells. However, the accumulations of heavy metal ions in environment within the approved environmental protection agency limits are highly challenging. Among all heavy metal ions, Hg^{2+} is extremely toxic owing to its lipophilic nature of organo-mercury (CH_3HgX) under environmental aqueous media [1-3]. Mercury ingestion could cause fatal damage to human central nervous and endocrine systems [4-5]. Due to its unique chemical properties and lethal effects on environment along with living organism, in recent years rapid, selective and sensitive detections of mercury ions are intriguing targets [6-10]. Consequently, myriads of chemosensors towards sensitive Hg^{2+} detections based on chelation-enhanced fluorescence [11-20] and fluorometric chemodosimeter [21-30] approaches have long been designed and discussed. However, conventionally most of those chemosensing probes in selective fluorometric detections of Hg^{2+} are suffered owing to a fact that fluorescence intensities of probe molecules could be altered by photo bleaching, concentration variations of probe ensembles and heterogeneities of surrounded microenvironments. Thus, developing Hg^{2+} selective optical indicators are highly demanding.

An exceptional electron-accepting capability of 3-cyano-4,5,5-trimethyl-2,5-dihydrofuran (TCF) make it as an excellent moiety for the applications of nonlinear optoelectronics [31-33]. However, its unique push-pull chromophoric nature stimulated scientists recently in designing novel red fluorophores for the applications of bioimaging- [34-37], pH sensing- [38,39], and chemosensing- [40-43] platforms, as well as dye sensitized solar cells (DSSCs) [44]. Liao et al. have demonstrated negative photo-chromism of a TCF chromophore [45]. Recently, Yu et al. have presented a near-infrared TCF-based probe for the colorimetric and ratiometric detection of

SO_2 [46]. Cho and co-workers have reported a selective optical TCF-based indicator for Hg^{2+} via an Hg^{2+} mediated intramolecular cyclization reaction of ethynyl phenols [47]. However, to the best our knowledge the selective and sensitive optical indicator based on the TCF moiety towards Hg^{2+} via chelation induced large hypsochromic shifted chemosensing ensemble has never been reported.

Herein, we demonstrate the first selective optical indicator **T2** towards Hg^{2+}, which was constructed by bridging an electron-withdrawing TCF moiety with a water soluble and well-known thiophilic ligand [48,49]. The utilization of the TCF moiety in this work as a strong electron-delocalizing unit via its flexible push-pull feature leads to an unprecedented sensing ensemble **T2**. It displays a 100% water solubility with surprisingly large blue-shifted photophysical properties of the selective detection towards Hg^{2+} via a H-type self-association and alterable ICT of the TCF moiety and yields a better live cell permeability as shown in scheme 1. Prominently, the selective detection of probe **T2** towards Hg^{2+} was completely reversible upon the addition of EDTA, which proves its practical utility.

2. Experimental Section

2.1. Materials

All chemicals and solvents were used are reagent grades and HPLC grades respectively and were purchased from Aldrich, ACROS, Fluka, TCI, TEDIA, and Lancaster Chemical Co. All chemicals were used without any further purification. Anhydrous solvents were obtained by passing through activated alumina column purification system, further dried by standard drying procedures. Solvents were degassed by freeze/thaw/pump cycle technique prior to use. Thin layer chromatographies (TLC) were performed on glass plate coated with silica 60 F24 (Merck).

The plates were visualized using ultra-violet light (256 nm) and developed using I_2 chamber. Flash chromatographies were performed on Merck silica gel 60 (230-400 mesh) under pressure using desired solvents.

2.2. General Characterization Methods

All reactions and operations were carried out under an atmosphere of inert argon or nitrogen using Schlenk techniques unless otherwise stated. ^{1}H NMR and ^{13}C NMR spectra were recorded on Bruker DRX-300 Avance series or on a Varian Inova 400, Inova 500, and Inova 600 Series (^{1}H: 300, 400, 500, and 600 MHz; ^{13}C: 75, 100, 125, and 150 MHz) at a constant temperature of 298 K. Chemical shifts were reported in parts per million from low to high field and referenced to residual solvent ($CDCl_3$, DMSO-d_6: ^{1}H δ = 7.26, 2.49 ppm and ^{13}C δ = 77.23, 39.52 ppm, respectively). Coupling constant (*J*) were reported in Hertz (Hz). UV-Vis spectra were recorded on the Jasco UV-600 spectrophotometer using 1 cm quartz cuvette. Fluorescence measurements were conducted with HITACHI 7000 Series Spectrophotometer. All emission and excitation spectra were corrected for the detector response and the lamp output. Melting points were determined using a Fargo MP-2D apparatus and are uncorrected. Elemental analyses were conducted on HERAEUS CHN-OS RAPID elemental analyzer. Time resolved photoluminescence (TRPL) spectra were measured using a home built single photon counting system with excitation from a 400 nm diode laser (Picoquant PDL-200, 50 ps fwhm, 2 MHz). The signals collected at the excitonic emissions of all sample solutions were connected to a time-correlated single photon counting card (TCSPC, Picoquant Timeharp 200). The emission decay data were analyzed for **T2** and complex **T2**-Hg with biexponential kinetics, from which two decay components were derived; the lifetime values of (τ1, τ2) and pre-exponential factors (A1, A2) were determined. Confocal imaging was carried out using Leica TCS SP8 confocal

fluorescence microscope, confocal fluorescence imaging with using 60 × times oil objective. Semi-empirical PM3 calculations were calculated using Gaussian-09 suite.

2.3. Cell Culture and Imaging

The human cervical cancer cell line (HeLa cells) were seeded onto cover slips at a concentration of (2 × 105 cells/mL) and cultured in Dulbecco's Modified Eagle's Medium (DMEM) and 10% fetal bovine serum in an incubator (37^{o}C, 5% CO_2, and 25% O_2). After 30 h, the cover slips were rinsed slightly 3 times with PBS to remove the media and then cultured in PBS for later use. In view of imaging procedure, initially cells were incubated with 5 µM of probe **T2** alone for 20 min at 37°C and observed under microscope and then again the samples were treated with $HgCl_2$ (10 µM) incubated for 20 min and then again observed under microscope and then the samples were treated with EDTA (10 µM) incubated for 20 min and moved to the confocal stage. All the samples were slightly rinsed for 3 times with PBS buffer before observing them under the microscope. All the cell images were obtained with Leica TCS SP8 confocal fluorescence microscope using 60 × times oil objective.

2.4. Stock Solutions

Standard solution of probe **T2** (100 mM) were prepared in double distilled water and $HgCl_2$, other metal ions stock solutions with concentration of (10 mM) were prepared, respectively in water. Before the titrations probe and analytes were diluted to their desired volumes.

Synthesis of Diethyl2,2'-((((4-formylphenyl)azanediyl)bis(ethane-2,1-diyl))bis(sulfanediyl))diacetate-(4). In a 25 mL dried round bottomed flask, sodium (0.48 g, 20 mmol) was added to anhydrous ethanol (12 mL). After sodium was dissolved completely, ethyl-2-mercaptoacetate (2.40 g, 23 mmol) was added dropwise. The mixture was stirred for 2 h at 40°C. Then a solution of 4-(bis (2-chloroethyl) amino) benzaldehyde (**3**) (2.24 g, 9 mmol) in

DMF (5 mL) was added. The stirring was continued for another 3 h. Water (20 mL) was added to the residual and extracted with dichloromethane (3 × 10 mL). The combined organic phase was washed twice with water and dried over anhydrous magnesium sulfate. The solvent was removed by evaporation and dried in vacuum, yielding a yellow oil of compound **4** (3.58 g, 95%). The structure of **4** was confirmed by ^{1}H NMR and ^{13}C NMR, which are shown as follows: ^{1}H NMR (500 MHz, CDCl3): δ 9.58 (s, 1H), 7.61 (d, *J* = 8.5 Hz, 2H), 6.63 (d, *J* = 9.0 Hz, 2H), 4.07 (q, *J* = 14.2 Hz, 4H), 3.56 (t, *J* = 7.5 Hz, 4H), 3.17 (s, 4H), 2.76 (t, *J* = 7.5 Hz, 4H), 1.16 (t, *J* = 7.0 Hz, 6H); ^{13}C NMR (125 MHz, CDCl3): δ 190.0, 170.1, 151.3, 132.0, 125.2, 110.7, 61.3, 50.23, 33.1, 28.9, 13.8.

Synthesis of (E)-Diethyl 2,2'-((((4-(2-(4-cyano-5-(dicyanomethylene)-2,2-dimethyl-2,5-dihydrofuran-3-yl)vinyl)phenyl)azanediyl)bis(ethane-2,1-diyl))bis(sulfanediyl))diacetate-(T1). Diethyl 2,2'-((((4-formylphenyl)azanediyl)bis(ethane-2,1-diyl))bis(sulfanediyl))diacetate-(**4**) (1.24 g, 3 mmol), 2-(3-cyano-4,5,5- trimethylfuran-2(5H)-ylidene)propanedinitrile (TCF) (0.6 g, 3 mmol), and ammonium acetate (0.23 g, 3 mmol) were stirred overnight in the dark at room temperature in a mixture of THF (10 mL) and EtOH (2.5 mL). The solution rapidly turns from pale yellow to reddish-orange. The mixture is diluted in water, extracted with ethyl acetate, washed with brine and dried over anhydrous $MgSO_4$. Evaporation of the solvents under reduced pressure yields a crude product that is purified by column chromatography on silica gel using progressively more polar 2:1 to 3:1 ethyl acetate: hexanes as the mobile phase to afford the desired **T1** red solid flakes (1.28 g, 72%). The structure of **T1** was confirmed by ^{1}H NMR and ^{13}C NMR, which are shown as follows: ^{1}H NMR (500 MHz, $CDCl_3$): δ 7.58 (d, *J* = 16.0 Hz, 1H), 7.54 (d, *J* = 8.5 Hz, 2H), 6.76 (d, *J* = 8.5 Hz, 2H), 6.74 (d, *J* = 16.0 Hz, 1H), 4.18 (q, *J* = 14.5 Hz, 4H), 3.67 (t, *J* = 7.0 Hz, 4H), 3.24 (s, 4H), 2.86 (t, *J* = 7.0 Hz, 4H), 1.73 (s, 6H), 1.26

(t, J = 7.0 Hz, 6H); ^{13}C NMR (125 MHz, $CDCl_3$): δ 176.1, 174.3, 170.1, 151.0, 148.0, 132.3, 122.6, 112.5, 112.3, 111.8, 111.2, 109.4, 97.0, 95.0, 61.5, 50.6, 33.5, 29.4, 26.6, 14.1; HRMS-ESI (m/z) calcd for $C_{30}H_{35}N_4O_5S_2$: 595.2049 $[M+H]^+$; found 595.2045; Anal. calcd for $C_{30}H_{34}N_4O_5S_2$: C, 60.58; H, 5.76; N, 9.42; found C, 60.51; H, 6.22; N, 9.46 (%).

Synthesis of Lithium (E)-2,2'-((((4-(2-(4-cyano-5-(dicyanomethylene)-2,2-dimethyl-2,5-dihydrofuran-3-yl)vinyl)phenyl)azanediyl)bis(ethane-2,1-diyl))bis(sulfanediyl))diacetate-(T2). A solution of **T1**-ester (416 mg, 0.7 mmol) in a 1:1 tetrahydrofuran/methanol mixture (50 mL) under a nitrogen atmosphere was cooled to 0°C and treated with 15 equiv. of lithium hydroxide. The resulting mixture was stirred for 2 days under nitrogen. Once hydrolysis was completed based on TLC THF-MeOH, the solvent was evaporated under reduced pressure and directly absorbed on short pad of silica and eluted in DCM-THF from 3:1 to 1:3 to get final **T2** salt. (323 mg, 84%). The structure of **T2** was confirmed by ^{1}H NMR, ^{13}C NMR, and elemental analysis, which are shown as follows: ^{1}H NMR (400 MHz, DMSO-d_6): δ 7.90 (d, J = 16.0 Hz, 1H), 7.75 (d, J = 9.2 Hz, 2H), 6.89 (d, J = 16.0 Hz, 1H), 6.85 (d, J = 8.8 Hz, 2H), 3.71 (t, J = 7.2 Hz, 4H), 3.27 (s, 4H), 2.81 (t, J = 7.2 Hz, 4H), 1.74 (s, 6H); ^{13}C NMR (100 MHz, DMSO-d_6): δ 177.3, 135.5, 151.5, 149.2, 133.1, 122.3, 113.5, 112.6, 112.2, 112.0, 108.6, 98.3 (2C), 92.5, 51.1, 50.2, 30.4, 28.7, 25.6; MS-ESI (m/z) calcd for $C_{26}H_{24}N_4O_5S_2$: 536.1 $[M-2Li]^-$; found 536.7; Anal. calcd for $C_{26}H_{24}Li_2N_4O_5S_2$: C, 56.73; H, 4.39; N,10.18; found C, 55.95; H, 4.44; N, 9.91 (%).

3. Results And Discussion

3.1. Synthesis

The synthetic route for **T2** was demonstrated in Scheme 2. Compounds 2,2'-(phenylazanediyl)diethanol (**2**) [50], 4-(bis(2-chloroethyl)amino)benzaldehyde (**3**) [51], and 2-(3-cyano-4,5,5-trimethylfuran-2(5H) ylidene)malononitrile(TCF) [50] were prepared according to literature procedures. Compound **3** was further reacted with 2-mercaptoacetic acid ethyl ester to afford diester **4** in 95% yield. Coupling of **4** and TCF gave **T1** in 72% yield. Ester hydrolysis of **T1** under basic conditions proceeds quantitatively to gave **T2**. The yielded compounds were characterized by using different spectroscopic methods, and the spectral data was shown in supporting information (Figs. S4-S9).

*3.2. UV-Visible and Fluorescence Measurements of Probe **T2***

Thanks to the lipophilic thiolate unit of **T2**, it possessed a complete water solubility, so we primarily assessed spectroscopic properties of probe **T2** (5 µM) in pure water, which showed a strong UV-absorption band cantered at 575 nm with purple color and a red-fluorescent band at 650 nm as shown in Fig. S1a and S1b, respectively. Interestingly, **T2** demonstrated excellent sensor selectivity in both UV-Vis and photoluminescence (PL) spectra upon the addition of Hg^{2+}, where the UV-absorption maximum was blue-shifted from 575 nm (purple color) to 405 nm (color less) and the red-fluorescence of **T2** was quenched as shown in Figures 1a and 1b, respectively. Furthermore, we screened both UV-Vis and PL changes of probe **T2** towards various metal ions, all of the other metal ions, including Li^{+}, Na^{+}, K^{+}, Cs^{+}, Cu^{+}, Ag^{+}, Mg^{2+}, Ca^{2+}, Ba^{2+}, Cu^{2+}, Zn^{2+}, Ni^{2+}, Fe^{2+}, Co^{2+}, Pb^{2+}, Cd^{2+}, Mn^{2+}, Ag^{2+}, Al^{3+}, Cr^{3+}, Fe^{3+}, and Eu^{3+}, could not induce considerable fluorescent changes.

By considering the vivid spectroscopic clue and to evaluate quantitative analysis of probe **T2**, we further measured both UV-Vis and PL changes of **T2** (5 µM) by increasing the concentration of Hg^{2+} from 0 to 10 µM. As shown in Fig. 2a, upon the addition of Hg^{2+} a sharp decline in the

absorption band at 575 nm and a simultaneous increase of newly blue-shifted band at 405 nm were observed. However, the fluorescence emission band at 650 nm was gradually decreased (Fig. 2b) and the stern-volmer plot denoted a dynamic fluorescence quenching of probe **T2** towards Hg^{2+}. The unusual nature of absorption ratiometric calibration curve at A574/A405 and the prominent hypsochromic shift in the absorption maxima of **T2** could be ascribed to the H-type self-association [53] of TCF moiety resulted from the coordination of Hg^{2+}. Furthermore, the observed isosbestic point at 468 nm clearly attested the aggregation of TCF moiety in the aqueous medium owing to its strong electron-withdrawing nature. Conventionally, strong electron acceptor dye molecules led to a depletion in quantum yields and imparts an unusual photophysical features [54,55]. The association constant was calculated to be 2.02×10^7 M^{-1} and 1:1 binding stoichiometry was estimated, which was based on the linear curve fitting for the fluorescence emission changes of probe **T2** supported by the Job's plot in the presence of Hg^{2+} (see Fig. 3).

3.3 Screening of Other Metal Ions and Naked Eye Color Change

Moreover, the color changes of naked-eye observation and fluorescence emission of **T2** towards metal ions are depicted in Fig. S2a and S2b. Moreover, to prove the specific selectivity of probe **T2** towards Hg^{2+} by single and dual metal studies, the effects of commonly encountered heavy metal ions on complex **T2-Hg** are evaluated as shown Fig. 4, where none of the tested metal ions could interfere with the detection process of Hg^{2+}. To gain the additional information about the binding modes operating in these recognition processes, ^{1}H NMR titration studies of probe **T2** upon the addition of Hg^{2+} as well as the reversibility of complex **T2**-Hg^{2+} with EDTA are also performed. The stacked ^{1}H-NMR spectra of probe **T2**, complex **T2**-Hg^{2+}, and **T2**+Hg(II)+EDTA are provided in Fig.5. Upon the addition of Hg^{2+} to the solution of **T2** in

CD_3CN-D_2O, large down-field shifts and broadening of proton peaks are observed in the aliphatic region of H_a, H_b, and H_c along with the aromatic region of H_d. These proton shifts of complex **T2**-Hg^{2+} are attributed to the shielding effect of complexation of **T2** and Hg^{2+}. However, a well-resolved spectrum of **T2**+Hg(II)+EDTA is almost identical with the ^1H NMR spectrum of **T2** itself after the treatment of complex **T2**-Hg^{2+} with EDTA. It confirms the specific detection and reversibility of probe **T2** towards Hg^{2+}. To our delight, both on-off-on fluorescence etiquettes and naked-eye color changes as shown in Fig. 6 were successfully achieved via the alternative addition of Hg^{2+} and EDTA up to 4 cycles.

3.4. Time Resolved Photoluminescence Measurements

To substantiate the aforementioned photophysical observations, time resolved fluorescence measurements were carried out for **T2**, **T2-Hg**, and recovered **T2** probed at 650 nm (λ_{ex} = 575 nm). The original mono-exponential decay of **T2** component with a life time of (τ1) 0.29 ns greatly transformed [56,57] into a marked biexponential decay with life time values of τ1 = 0.32 ns (94.35%) and τ2 = 25.12 ns (5.65%) in the presence of Hg^{2+} as shown in Fig. S3. Biexponential life time components could be ascribed to the chelation of probe with Hg^{2+} to induce the intrinsic fluorescence quenching of TCF. However, the further addition of EDTA to **T2-Hg** yielded a mono-exponential decay component with the life time value of 0.26 ns, which evidenced the complete reversibility of probe **T2**.

3.5. Theoretical Studies

To rationalize the coordination of Hg^{2+} with **T2** induced by ICT quenching process, it has been carried out by using the density functional theory (DFT) method to further support the experimental observation of ligand and metal interaction. All calculations were carried out using the Gaussian 09 package [58]. The electronic ground state geometry optimization of **T2** with

charge -2 and neutral complex **T2-Hg** were carried out by using the M06-2X method. The basis set used in this calculation is Lanl2dz, which includes the D95 double-ξ basis set for Hg along with Hay and Wadt's effective core potential (ECP) and the 6-31G(d) basis set for main group elements. We also calculated the frontier molecular orbitals at the same level of theory. As shown in Fig. 7, the most stable optimized geometries of **T2** and complex **T2-Hg** along with its marked bond lengths were attested the strong Hg^{2+} coordination within the lipophilic thiolated ligand. As anticipated, both of the ground states HOMO and HOMO-1 molecular distributions of **T2** were mainly resided on thiophilic ligand part as shown in Fig. 8a. Whereas, both LUMO and LUMO+1 molecular orbital distributions were mainly vested on TCF moiety (see Fig. 8b) donated strong intramolecular charge transfer distribution between aniline thiophilic ligand to TCF moiety. However, with the addition of Hg^{2+} both ground state HOMO and LUMO level distributions existed on TCF and π-bridge, and next excited state HOMO-1 and LUMO+1 were shifted to Hg^{2+}coordinated thiophilic ligand part, which clearly denoted the effective obstruction of ICT within complex **T2-Hg**, as shown in Fig. 9a and 9b, respectively. Based on these concrete experimental and theoretical results, we inferred that probe **T2** could selectively detect Hg^{2+} without any interference from common heavy metals and act as a useful Hg^{2+} selective optical indicator.

3.6. Confocal Imaging

We next sought to apply current probe **T2** in living cells, stimulated by its described photophysical characteristics. As shown in Figs. 10a-10c denoted red fluorescence, the cells were incubated with probe **T2** (5 μM) alone for 20 min at 37°C. However, a noticeable fluorescence quenching in Figs. 10d-10f was monitored in the cells after the treatment with Hg^{2+} (10 μM). As shown in Figs. 10g-10i, the red fluorescence was restored in the cells upon further

treatment with EDTA. Noticeable changes signified that probe **T2** was cell membrane permeable and capable of selective imaging of Hg^{2+} in the living cells.

4. Conclusions

In conclusion, we have developed a selective and sensitive red fluorescent probe for the detection of Hg^{2+} based on thiophilic ligand connected to a push-pull active TCF moiety under 100% aqueous medium. Exclusively, probe **T2** showed a selective colorimetric response with unprecedented and exceedingly large hypsochromic shift (170 nm) in absorption of **T2** induced by the aggregation of TCF coordinated with Hg^{2+} in aqueous medium. Current probe showed a stable colorimetric and ratiometric response towards Hg^{2+} over a range of tested transition and other metal ions, where the UV-absorption maximum was blue-shifted from 575 nm (purple color) to 405 nm (color less) and the red-fluorescence emission band at 650 nm was quenched, respectively. Furthermore, the optimized geometries of **T2** and **T2-Hg** ensembles via the energy minimized and density functional theory (DFT) methods fortified the intramolecular charge transfer (ICT) mechanism between the probe and TCF unit. Pivotal confocal imaging of **T2** and **T2-Hg** in living cells also demonstrated that probe **T2** could be favorable for biological applications. Besides, invincible absorption changes and fluorescence quenching spectral appearances allowed us to present the selective optical indicator of Hg^{2+} via H-type aggregation of TCF moiety for the first time.

Acknowledgements

We thank the Ministry of Science and Technology (MOST) in Taiwan for the financial supports of this project through MOST 103-2113-M-009-018-MY3 and MOST 103-2221-E-009-215-MY3.

References

[1] Nolan EM, Lippard SJ. Tools and tactics for the optical detection of mercuric ion. Chem Rev 2008; 108: 3443–80.

[2] Boening DW. Ecological e ects, transport, and fate of mercury: a general review Chemosphere 2000; 40: 1335–51.

[3] Ullrich SM, Tanton TW, Abdrashitova SA. Mercury in the aquatic environment: a review of factors affecting methylation. Crit Rev Environ Sci Technol 2001; 31: 241–93.

[4] Benoit JM, Fitzgerald WF, Damman AWH. The biogeochemistry of an ombrotrophic bog: evaluation of use as an archive of atmospheric mercury deposition. Environ Res 1998; 78: 118–33.

[5] Kuwabara JS, Arai Y, Topping BR, Pickering AIJ, George GN. Mercury speciation in piscivorous fish from mining-impacted reservoirs. Environ Sci Technol 2007; 41: 2745–49.

[6] Desvergne JP, Czarnik AW. Eds. Chemosensors of ion and iolecule recognition. Kluwer: Dordrecht; 1997.

[7] Czarnik AW. Eds. Fluorescent chemosensors for ion and molecule recognition. American Chemical Society Washington DC; 1992.

[8] Mercury update: Impact on fish advisories, EPA fact sheetEPA-823-F-01-011, EPA, Office of water. Washington DC; 2001.

[9] Kim YR, Mahajan RK, Kim JS, Kim H. Highly sensitive gold nanoparticle-based colorimetric sensing of mercury (II) through simple ligand exchange reaction in aqueous media. ACS Appl Mater Interfaces 2010; 2: 292–95.

[10] Hussain S, De S, Iyer PK. Thiazole-containing conjugated polymer as a visual and fluorometric sensor for iodide and mercury. ACS Appl Mater Interfaces 2013; 5: 2234−40.

[11] Cheng X, Li Q, Qin J, Li Z. A new approach to design ratiometric fluorescent probe for mercury (II) based on the Hg^{2+}-promoted deprotection of thioacetals. ACS Appl Mater Interfaces 2010; 2: 1066–72.

[12] Xin DJ, Jiuli Z, Qian L, Chang LS, Jian G, Gao TS, Lin JX. Synthesis of NIR fluorescent thienyl-containing aza-BODIPY and its application for detection of Hg^{2+}: Electron transfer by bonding with Hg^{2+}. Dyes and Pigments 2016; 125: 136-41.

[13] Srivastava P, Razi SS, Ali R, Gupta RC, Yadav SS, Narayan G, Misra, A. Selective naked-eye detection of Hg^{2+} through an efficient turn-on photoinduced electron transfer fluorescent probe and its real applications. Anal Chem 2014; 86: 8693−99.

[14] Quang DT, Kim JS. fluoro- and chromogenic chemodosimeters for heavy metal ion detection in solution and biospecimens. Chem Rev 2010; 110: 6280–301.

[15] Zhu M, Yuan M, Liu X, Xu J, Lv J, Huang C, Liu H, Li Y, Wang S, Zhu D. Visible near-infrared chemosensor for mercury ion. Org Lett 2008; 10: 1481–84.

[16] Yuan M, Li Y, Li J, Li C, Liu X, Lv J, Xu J, Liu H, Wang S, Zhu D. A colorimetric and fluorometric dual-modal assay for mercury ion by a molecule. Org Lett 2007; 9: 2313–16.

[17] Neupane L, Park JY, Park JH, Lee KH. Turn-on fluorescent chemosensor based on an amino acid for Pb (II) and Hg (II) ions in aqueous solutions and role of tryptophan for sensing. Org Lett 2013; 15: 254–57.

[18] Satapathy R, Wu YH, Lin HC. Novel thieno-imidazole based probe for colorimetric detection of Hg^{2+} and fluorescence turn-on response of Zn^{2+}. Org Lett 2012; 14: 2564–67.

[19] Nguyen KH, Nguyen CB, Nguyen TAN, Nguyen TT, Pham CN, Tran D, Jong SK, Duong TQ. A highly sensitive fluorescent chemosensor for simultaneous determination of Ag (I), Hg (II), and Cu (II) ions: Design, synthesis, characterization and application. Dyes and Pigments 2015; 116: 89–96.

[20] Mian W, Jing W, Zhaohai Q, Hongmei W. A new coumarinerhodamine FRET system as an efficient ratiometric fluorescent probe for Hg^{2+} in aqueous solution and in living cells. Dyes and Pigments 2015; 120: 208–12.

[21] Du J, Fan J, Peng X, Sun P, Wang J, Li H, Sun SA. a new fluorescent chemodosimeter for Hg^{2+}: selectivity, sensitivity, and resistance to Cys and GSH. Org Lett 2010; 12: 476−79.

[22] Lee H, Kim HJ. Ratiometric fluorescence chemodosimeter for mercuric ions through the Hg (II)-mediated propargyl amide to oxazole transformation. Bull Korean Chem Soc 2011; 32: 3959–62.

[23] Lee H, Kim HJ. Ratiometric fluorescence chemodosimeter for mercuric ions through the Hg (II)-mediated propargyl amide to oxazole transformation. Tetrahedron Lett 2011; 52: 4775–78.

[24] Zhou Y, Zhu CY, Gao XS, You XY, Yao C. Hg^{2+}-selective ratiometric and "off−on" chemosensor based on the azadiene−pyrene derivative. Org Lett 2010; 12: 2566–69.

[25] Zhao Q, Li FY, Huang C. Phosphorescent chemosensors based on heavy-metal complexes. Chem. Soc Rev 2010; 39: 3007–30.

[26] Zhao Q, Huang C, Li FY. Phosphorescent heavy-metal complexes for bioimaging. Chem Soc Rev 2011; 40: 2508–24.

[27] Ma X, Wang J, Shan Q, Tan Z, Wei G, Wei D, Du YA. "Turn-on" fluorescent Hg^{2+} chemosensor based on ferrier carbocyclization. Org Lett 2012; 14: 820–23.

[28] Yang MH, Thirupathi P, Lee KH. Selective and sensitive ratiometric detection of Hg (II) ions using a simple amino acid based sensor. Org Lett 2011; 13: 5028–31.

[29] Sait M, Serkan E. A novel perylene-bisimide dye as "turn on" fluorescent sensor for Hg^{2+} ion found in DMF/H_2O. Dyes and Pigments 2015; 113: 763–69.

[30] Huan HW, Lin X, Cai LY, Yuan YQ, Hua J. Rhodamine-based fluorescent sensor for mercury in buffer solution and living cells. Dyes and Pigments 2011; 91: 350–55.

[31] Cabanetos C, Bentoumi W, Silvestre V, Blart E, Pellegrin Y, Montembault V, Barsella A, Dorkenoo K, Bretonnière Y, Andraud C, Mager L, Fontaine L, Odobel F. New cross-linkable polymers with huisgen reaction incorporating high μβ chromophores for second-order nonlinear optical applications. Chem Mater 2012; 24: 1143−57.

[32] Wu J, Bo S, Liu J, Zhou T, Xiao H, Qiu L, Zhen Z, Liu X. Synthesis of novel nonlinear optical chromophore to achieve ultrahigh electro-optic activity. Chem Commun 2012; 48: 9637–39.

[33] Yang Y, Xu H, Liu F, Wang H, Deng G, Si P, Huang H, Bo S, Liu J, Qiu L, Zhen Z, Liu X. Synthesis and optical nonlinear property of Y-type chromophores based on double-donor structures with excellent electro-optic activity. J Mater Chem C 2014; 2: 5124–32.

[34] Lord SJ, Conley NR, Lee HLD, Samuel R, Liu N, Twieg RJ, Moerner WE. A photoactivatable push−pull fluorophore for single-molecule imaging in live cells. J Am Chem Soc 2008; 130: 9204–05.

[35] Bouffard J, Kim Y, Swager TM, Weissleder R, Hilderbrand SA. A highly selective fluorescent probe for thiol bioimaging. Org Lett 2008; 10: 37–40.

[36] Lee HLD, Lord SJ, Iwanaga S, Zhan K, Xie H, Williams JC, Wang H, Bowman GR, Goley ED, Shapiro L, Twieg RJ, Rao J, Moerner WE. Superresolution imaging of targeted proteins in fixed and living cells using photoactivatable organic fluorophores. J Am Chem Soc 2010; 132: 15099–10.

[37] Lee MK, Williams J, Twieg RJ, Rao J, Moerner WE. Chem Sci 2013; 4: 220–25.

[38] Jin Y, Tian Y, Zhang W, Jang SH, Jen AKY, Meldrum DR. Tracking bacterial infection into macrophages by a novel red-emission pH sensor. Anal Bioanal Chem 2010; 398: 1375–84.

[39] Ipuy M, Billon C, Micouin G, Samarut J, Andraud C, Bretonnière C. Fluorescent push–pull pH-responsive probes for ratiometric detection of intracellular pH. Org Biomol Chem 2014; 12: 3641–48.

[40] Chen T, Zheng Y, Xu Z, Zhao M, Xu Y, Cui J. A red emission fluorescent probe for hydrogen sulfide and its application in living cells imaging. Tetrahedron Lett 2013; 54: 2980–82.

[41] Gwon SY, Kim SH. Anion sensing and F-induced reversible photoreaction of D-p-A type dye containing imidazole moiety as donor. Spectrochimica Acta Part A Molecular and Biomolecular Spectroscopy 2014; 117: 810–13.

[42] Park J, Kim H, Choi Y, Kim Y. A ratiometric fluorescent probe based on a BODIPY–DCDHF conjugate for the detection of hypochlorous acid in living cells. Analyst 2013; 138: 3368–71.

[43] Zhou X, Su F, Tian Y, Youngbull C, Johnson RH, Meldrum DR. A new highly selective fluorescent K^+ sensor. J Am Chem Soc 2011; 133: 18530–33.

[44] Hao Y, Yang X, Cong J, Tian H, Hagfeldt A, Sun L. Efficient near infrared D–π–A sensitizers with lateral anchoring group fordye-sensitized solar cells. Chem Commun 2009; 4031–33.

[45] Peng P, Strohecker D, Liao Y. Negative photochromism of a TCF chromophore. Chem Commun 2011; 47: 8575–77.

[46] Wu MY, Li K, Li CY, Hou JT, Yu XQ. A water-soluble near-infrared probe for colorimetric and ratiometric sensing of SO2 derivatives in living cells. Chem Commun 2014; 50: 183–85.

[47] Atta AK, Kim SB, Heo J, Cho DG. Hg (II)-mediated intramolecular cyclization reaction in aqueous media and its application as Hg (II) selective indicator. Org Lett 2013; 15: 1072–75.

[48] Zhao Y, Lv X, Liu Y, Liu J, Zhang Y, Shi H, Guo W. The emission enhancement of the NIR distyryl bodipy dyes by the indirect S0-S2 excitation and their application towards a Hg^{2+} probe. J Mater Chem 2012; 22: 11475–78.

[49] Hiruta Y, Koiso H, Ozawa H, Sato H, Hamada K, Yabushita S, Citterio D, Suzuki K. Near IR emitting red-shifting ratiometric fluorophores based on borondipyrromethene. Org Lett 2015; 17: 3022−25.

[50] Lin SW, Sun Q, Ge ZM, Wang X, Ye J, Li RT. Synthesis and structure–analgesic activity relationships of a novel series of monospirocyclopiperazinium salts (MSPZ). Bioorg Med Chem Lett 2011; 21: 940–43.

[51] Massin J, Dayoub W, Mulatier JC, Aronica C, Bretonniere Y, Andraud C. Near-infrared solid-state emitters based on isophorone: synthesis, crystal structure and spectroscopic properties. Chem Mater 2011; 23: 862–73.

[52] Zhang T, Guo KP, Qiu L, Shen Y. magnesium ethoxide as an effective catalyst in the synthesis of dicayanomethylendihydrofurans. Synthetic Communications 2006; 36:1367–72.

[53] Zheng H, Zhang XJ, Cai X, Bian QN, Yan M, Wu GH, Lai XW, Jiang YB. Ratiometric fluorescent chemosensor for Hg^{2+} based on heptamethine cyanine containing a thymine moiety. Org Lett 2012; 14: 1986–89.

[54] Gopalan P, Katz HE, McGee DJ, Erben C, Zielinski T, Bousquet D, Muller D, Grazul J, Olsson Y. Star-shaped azo-based dipolar chromophores: design, synthesis, matrix compatibility, and electro-optic activity. J Am Chem Soc 2004; 126: 1741–47.

[55] Liao Y, Bhattacharjee S, Firestone, KA, Eichinger BE, Paranji R, Anderson CA, Robinson BH, Reid PJL, Dalton R. Antiparallel-aligned neutral-ground-state and zwitterionic chromophores as a nonlinear optical material. J Am Chem Soc 2006; 128: 6847–53.

[56] Raju MVR, Lin HC. A novel diketopyrrolopyrrole (DPP)-based [2] rotaxane for highly selective optical sensing of fluoride. Org Lett 2013; 15: 1274−77.

[57] Raju MVR, Prakash EC, Chang HC, Lin HC. A facile ratiometric fluorescent chemodosimeter for hydrazine based on ingemanske hydrazinolysis and its applications in living cells. Dyes and Pigments 2014; 103: 9–20.

[58] Frisch, M. J. et al, Gaussian, Inc: Wallingford CT; 2009.

Schemes and List of Figures

Scheme 1. Proposed sensing mechanism of **T2** towards Hg^{2+}.

Scheme 2. Synthetic route of probe **T2**.

(a) $ClCH_2CH_2OH$, $CaCO_3$, KI, H_2O, reflux 8 h, 86%; (b) $POCl_3$, dry DMF, 40°C, 8 h, 95%; (c) ethyl 2-mercaptoacetate, NaOEt, DMF, 40°C, 6 h, 95%; (d) TCF, NH_4OAc, EtOH/THF, rt, 30 h, 72%; (e) LiOH, THF/MeOH, rt, 2 day, 84%.

Fig. 1. (a) UV-Visible and (b) PL spectra of **T2** (5 μM) towards various metal ions in aqueous solutions. Bottom red line: in the presence of Hg^{2+} (10 μM) and the other metal ions (10 μM) Li^+, Na^+, K^+, Cs^+, Cu^+, Ag^+, Mg^{2+}, Ca^{2+}, Ba^{2+}, Cu^{2+}, Zn^{2+}, Ni^{2+}, Fe^{2+}, Co^{2+}, Pb^{2+}, Cd^{2+}, Mn^{2+}, Ag^{2+}, Al^{3+}, Cr^{3+}, Fe^{3+}, and Eu^{3+}, in aqueous solution. λ_{ex}= 570 nm. Insets are naked eye and PL photographs of **T2** (5 μM) in the absence and presence of Hg^{2+} (10 μM).

Fig. 2. (a) UV-Visible and (b) PL spectra of **T2** (5 μM) in aqueous solution upon the titration of Hg^{2+} (0 to 10 μM). (Inset) Stern-Volmer plot of I/I0 (λ_{em} = 650 nm) vs. [Hg^{2+}]. λ_{ex} = 570 nm.

Fig. 3. Calculation of association constant for complex **T2-Hg^{2+}** using Connors method.

Fig. 4. Emission intensity of **T2** (5 μM) at 650 nm. Black bars: free probe **T2**, or treated with the marked metal ions (20 equiv). Red bars: treated with the marked metal ions (20 equiv) followed by 2 equiv Hg^{2+} (λ_{ex} = 570 nm).

Fig. 5. ^{1}H-NMR (300 MHz) spectral changes of probe **T2**, complex **T2**-Hg^{2+}, and **T2**+Hg^{2+}+EDTA in CD_3CN-D_2O (1:1, v/v). Inset: proposed binding and recovery modes of complex **T2**-Hg^{2+} and **T2**+Hg^{2+}+EDTA, respectively.

Fig. 6. (a) Absorption and (b) emission spectral changes of **T2** (5μM), after addition of Hg^{2+} (10 μM) and followed by EDTA (10 μM). (c) Naked eye color changes of **T2** by adding Hg^{2+} followed by EDTA. (d) Fluorescence intensity changes of **T2** (5 μM) at 650 nm under addition of alternate compounds (Hg^{2+} and EDTA) for 4 cycles (λ_{ex} = 570 nm).

Fig. 7. Optimized geometries of probe **T2** anion and complex **T2-Hg** calculated using the B3LYP/Lanl2dz level. Bond lengths are in angstroms.

Fig. 8. Frontier molecular orbital distributions of probe **T2** caluculated by semi-empirical PM3 optimized (a) HOMO and (b) LUMO levels, respectively.

Fig. 9. Frontier molecular orbitals of complex **T2-Hg** based on optimal geometry, which is calculated at the B3LYP/Lanl2dz+6-31G(d) level .

Fig. 10. Confocal fluorescence images of hela cells. Top, (a-c) cells were incubated with probe **T2** (5 μM) for 20 min. Middle, (d-f) cells were then further incubated with Hg^{2+} (10 μM) for 20 min. Bottom, (g-i) cells were further treated with **EDTA** (10 μM) for 20 min. Bright field (a, d, and g), fluorescence (b, e, and h), and merged field (c, f, and i). λ_{ex} = 570 nm.

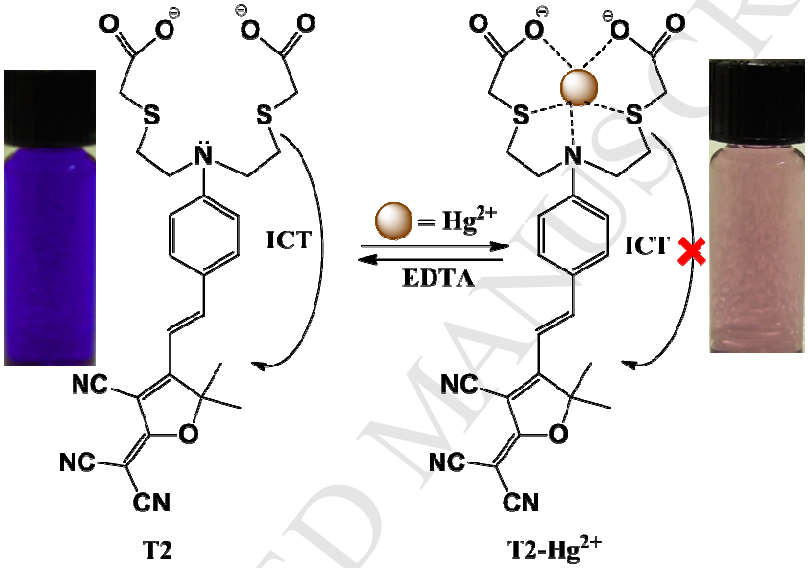

Scheme 1.

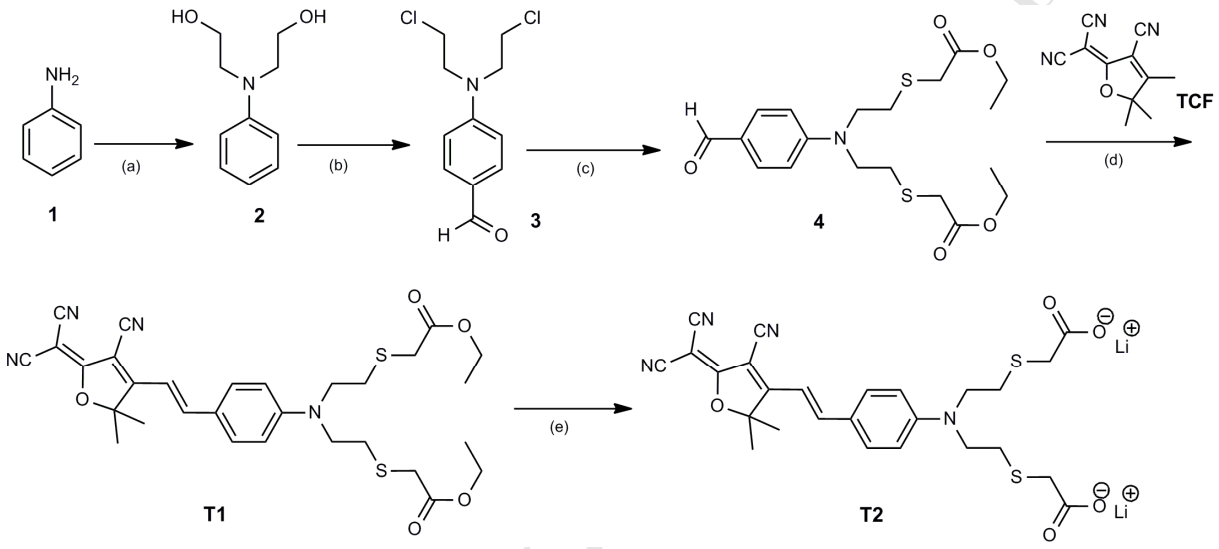

Scheme 2.

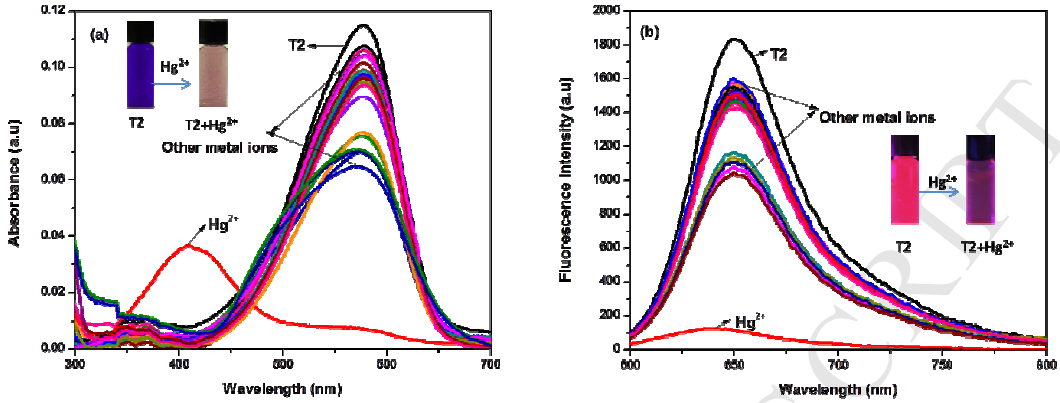

Fig. 1.

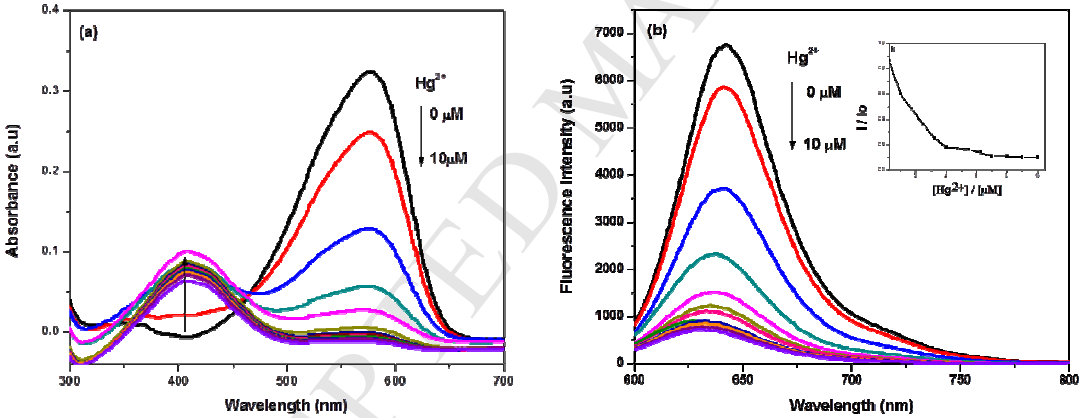

Fig. 2.

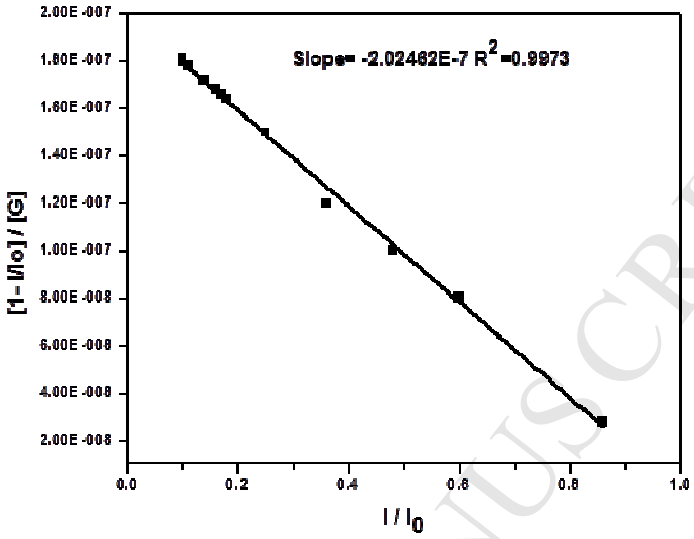
Slope= -2.02462E-7 R2=0.9973
[1- I/Io] / [G]
I / I0
2.00E-007
1.80E-007
1.60E-007
1.40E-007
1.20E-007
1.00E-007
8.00E-008
6.00E-008
4.00E-008
2.00E-008
0.0
0.2
0.4
0.6
0.8
1.0

Fig. 3.

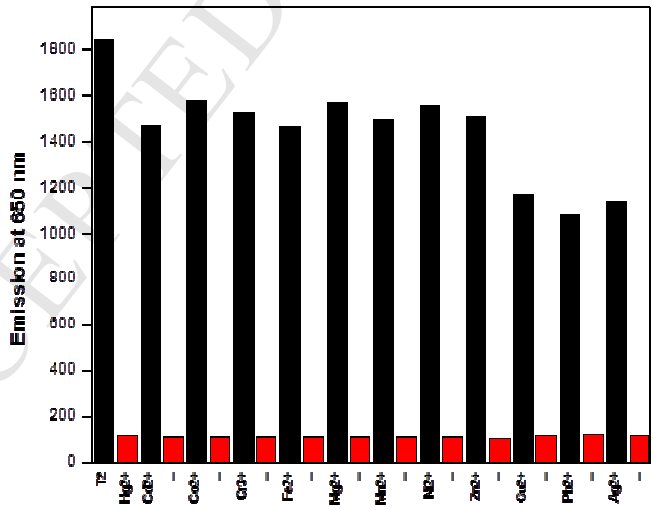
Emission at 650 nm
1800
1600
1400
1200
1000
800
600
400
200
0

Fig. 4.

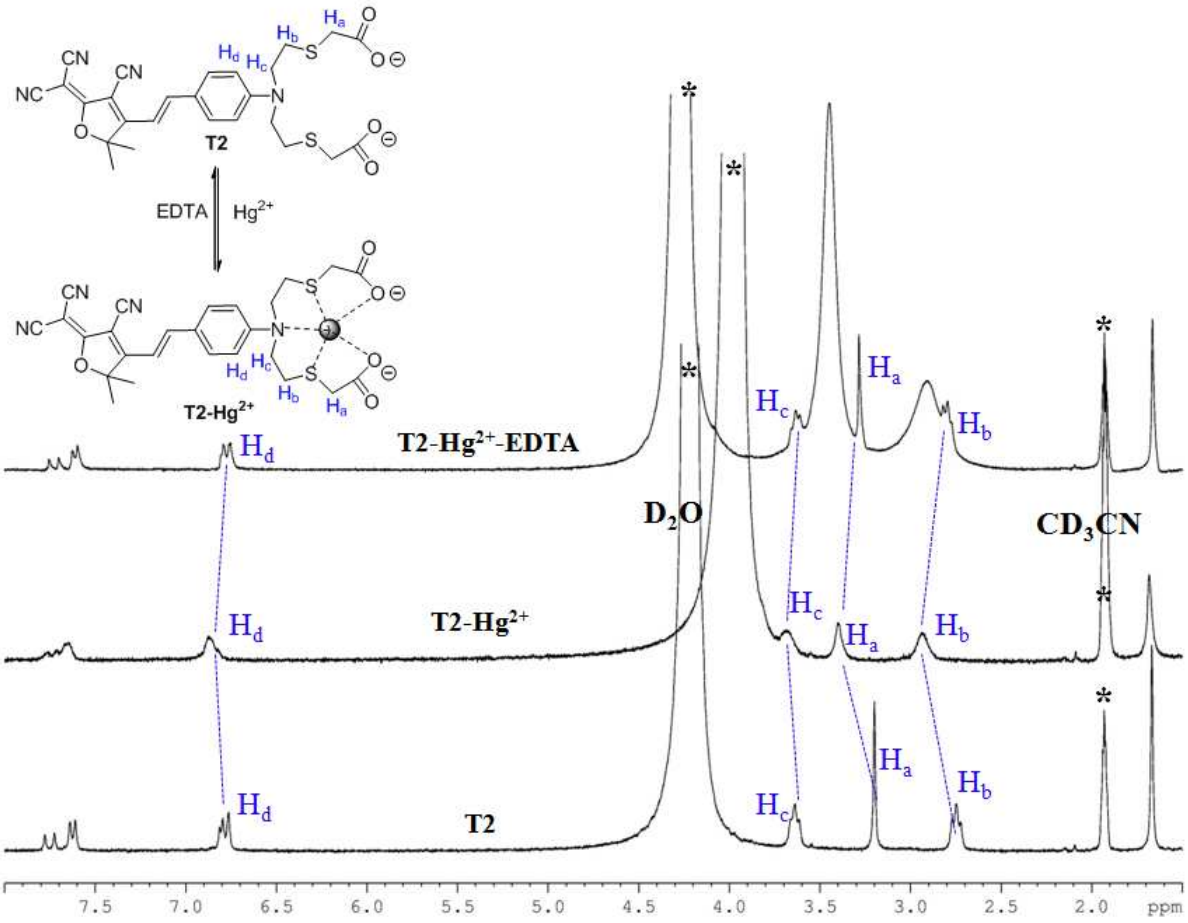

Fig. 5.

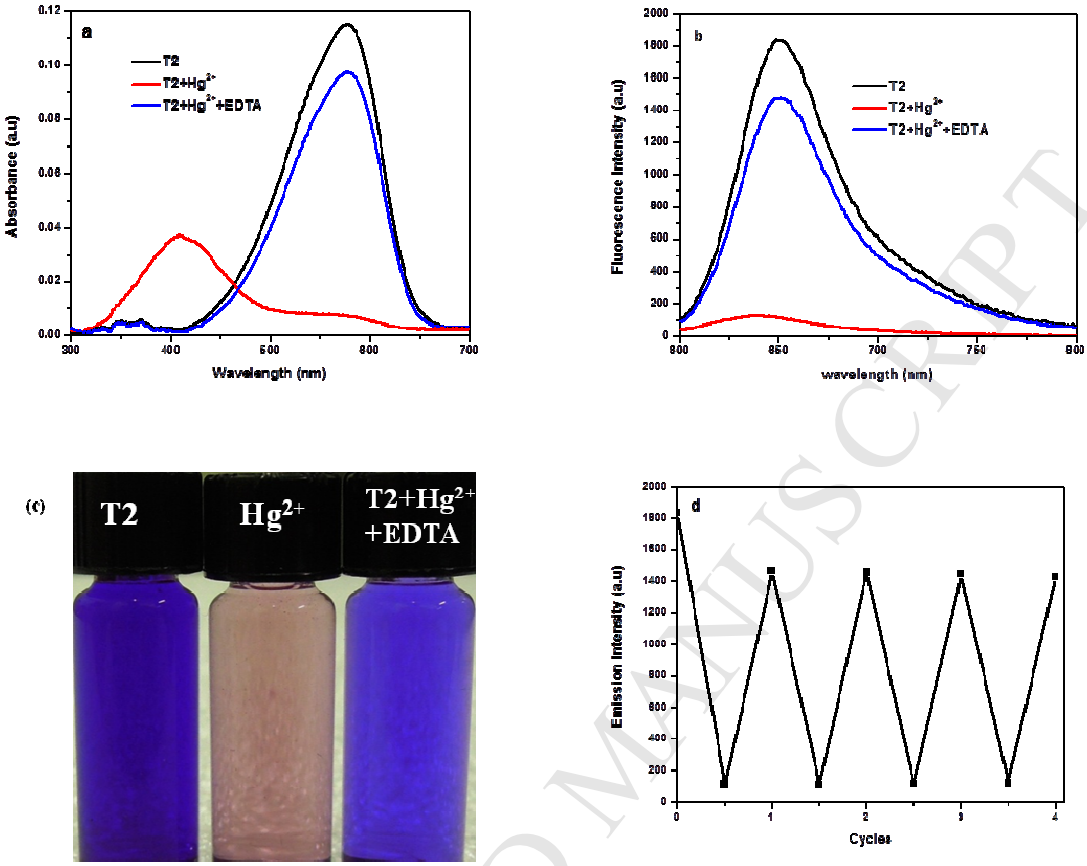

Fig. 6.

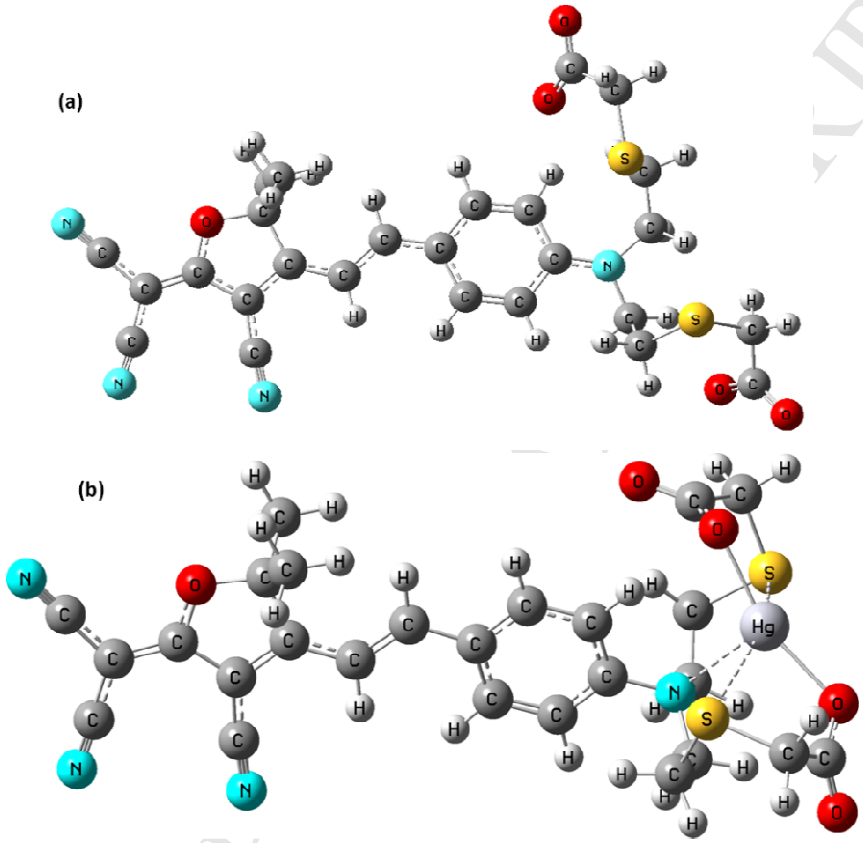

Fig. 7.

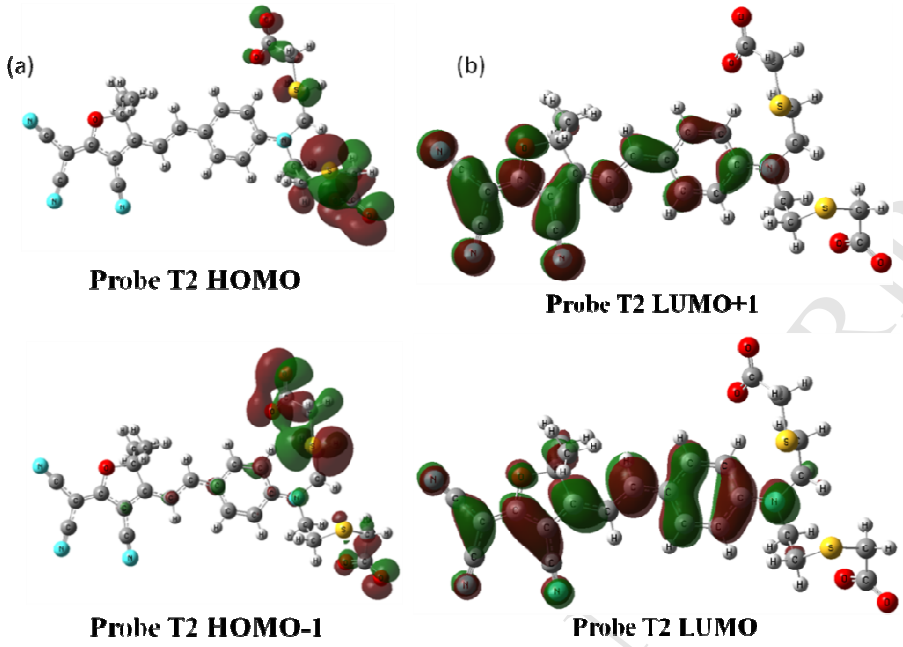
(a)
(b)
Probe T2 HOMO
Probe T2 LUMO+1
Probe T2 HOMO-1
Probe T2 LUMO

Fig. 8.

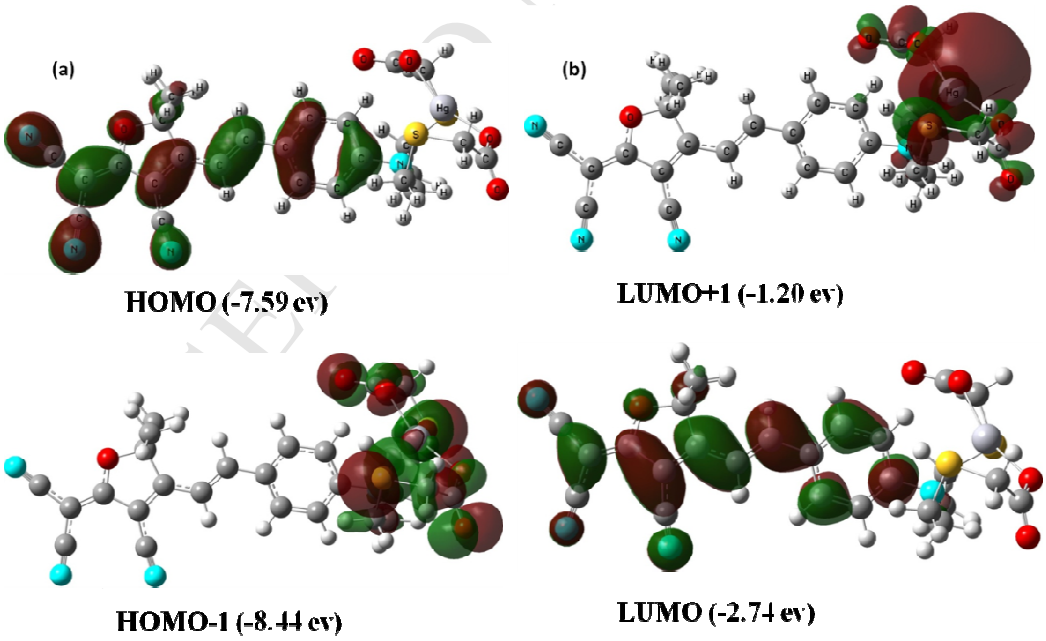
(a)
(b)
HOMO (-7.59 ev)
LUMO+1 (-1.20 ev)
HOMO-1 (-8.44 ev)
LUMO (-2.74 ev)

Fig. 9.

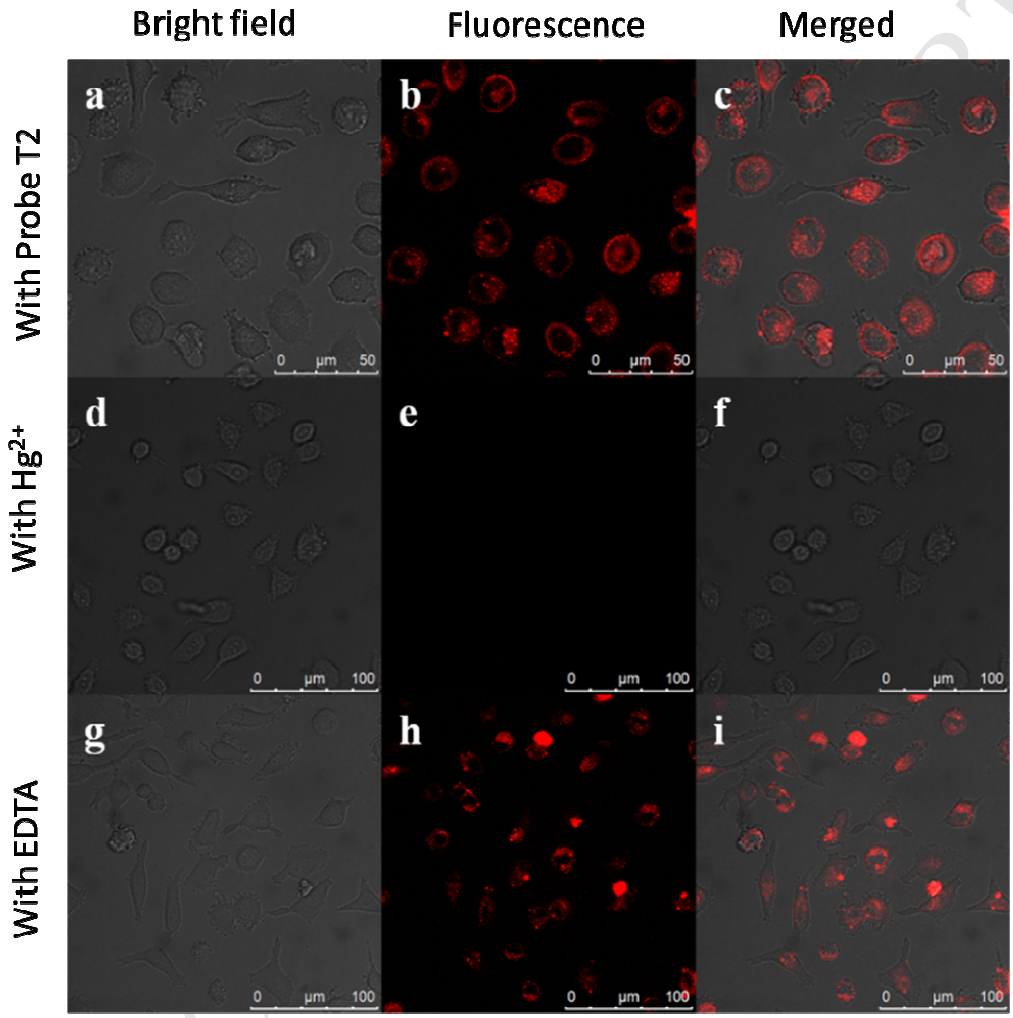
Bright field
Fluorescence
Merged
With Probe T2
With Hg2+
With EDTA
a
b
c
d
e
f
g
h
i
0 μm 50
0 μm 100

Fig. 10.

Highlights

- A water soluble and reversible Hg^{2+} ion sensor probe is synthesized.
- This probe works as a colorimetric and naked-eye sensor towards Hg^{2+} ion.
- A large blue shift is observed in absorption of the probe coordinated with Hg^{2+}.
- This probe has the optical sensor potential to be used in living cell applications.